SAND99-1984 J

Investigation of rising-sun magnetrons operated at relativistic voltages using three dimensional particle-in-cell simulation

R. W. Lemke

Sandia National Laboratories, Albuquerque, New Mexico 87185-1186

T. C. Genoni

Mission Research Corporation, , Albuquerque, New Mexico 87106

T. A. Spencer

Air Force Research Laboratory, Kirtland AFB, NM 87117

(Received

This work is an attempt to elucidate effects that may limit efficiency in magnetrons operated at relativistic voltages (V ~ 500 kV). Three-dimensional particle-in-cell simulation is used to investigate the behavior of 14 and 22 cavity, cylindrical, rising-sun magnetrons. Power is extracted radially through a single iris located at the end of every other cavity. Numerical results show that in general output power and efficiency increase approximately linearly with increasing iris width (decreasing vacuum Q) until the total Q becomes too low for stable oscillation in the π-mode to be maintained. Beyond this point mode competition and/or switching occur and efficiency decreases. Results reveal that the minimum value of Q (maximum efficiency) that can be achieved prior to the onset of mode competition is significantly affected by the magnitude of the 0-space-harmonic of the π-mode, a unique characteristic of rising-suns, and by the magnitude of the electron current density (space-charge effects). By minimizing these effects, up to 3.7 GW output power has been produced at an efficiency of 40%.

PACS 84.40.F

I. INTRODUCTION

The magnetron oscillator[1] can be a highly efficient device for generating microwaves. When operated at low voltage ($V < 100$ kV) efficiencies greater than 50% can be achieved.[2,3] At relativistic voltages (V~500 kV), however, the peak efficiency tends to be much less than 30%.[4-10] There is no definitive explanation for the low efficiency of relativistic magnetrons relative to commercial magnetrons. This work is an attempt to elucidate effects that may limit efficiency in magnetrons operated at relativistic voltages.

To this end we use three-dimensional (3D), particle-in-cell (PIC) simulation to model rising-sun magnetrons. We focus on the rising-sun because it is considered to be the most practicable configuration for achieving mode control at high voltage. Previous investigations of the relativistic magnetron suggest that 3D PIC simulation is capable of accurately modeling experimentally observed behavior.[11,12] Thus, by considering only practicable configurations the intent here is to produce results that are likely to be born out in an analogous experiment.

In this study the 3D, fully electromagnetic, PIC code QUICKSILVER[13] is used to investigate the behavior of 14 and 22 cavity, cylindrical, rising-sun magnetrons, which we respectively refer to as N14 and N22. The N14 is used to investigate effects of the 0-space-harmonic of the π-mode on magnetron performance, and the N22 is used explore space-charge effects.

In each configuration power is extracted radially through a single iris located at the end of every other cavity. Numerical results show that in general output power and efficiency increase approximately linearly with increasing iris width (decreasing vacuum Q) until the total Q becomes too low for stable oscillation in the π-mode to be maintained. Beyond this point mode competition and/or switching occur and efficiency decreases. Results reveal that the minimum value of Q that can be achieved prior to the onset of mode competition (i.e. maximum efficiency)

is significantly affected by the magnitude of the 0-space-harmonic of the π-mode, a unique characteristic of rising-suns, and by the magnitude of the electron current density (space-charge effects). By minimizing these effects, up to 3.7 GW output power has been produced at an efficiency of 40%.

The effects that 0-harmonic contamination and space charge can have on magnetron performance were discovered early on in magnetron research.[14,15] Using 3D PIC simulation we are able to quantify these phenomena and show how they are manifest at relativistic voltages.

This paper is organized as follows. To understand the behavior of rising-sun magnetrons one must understand the electromagnetic properties of this configuration. A summary of these properties is provided in Sec II. The simulation model, procedure, and results for the N14 and N22 configurations are presented in Sec. III. Section IV contains conclusions and recommendations derived from this investigation.

II. RISING-SUN ELECTROMAGNETICS

The electromagnetic characteristics of the rising-sun magnetron[16] can be understood through the dispersion relation for transverse electric (TE) modes. For this purpose we calculate the dispersion relation for the N14 configuration. The N14 is shown schematically in Fig. 1. The geometry is cylindrical and azimuthally symmetric. There are 14 cavities. (Note that some labels and parts of the figure pertain to simulation, and will be discussed in that context.)

Figure 1(a) is a cross section in the rz plane at a θ location corresponding to the azimuthal center of a deep cavity. Figures 1(b) and 1(c) are cross sections in the rθ plane at z locations of 0.3 m and 0.4 m (through an iris), respectively. The azimuthal width of each cavity is 2/3 the period.

All shallow cavities are closed, and all deep cavities are connected through an iris to an output sectoral waveguide (horn). Irises extend the full cavity width in θ. The outlet boundary [Fig.

1(a)] impedance is matched to the impedance of the radiated wave. This extraction technique was chosen to minimize the power flux per output waveguide. Note that for uniform cavities, opening every other cavity for extraction purposes creates a rising-sun-like configuration with similar dispersion characteristics.

In Fig. 1 the thick, solid lines outline the cathode and anode, which are assumed to be perfectly conducting. The cathode radius and axial length are r_c=0.073 m and L_c=0.208 m, respectively. The anode inner radius and axial length are r_a=0.097 m and L_a=0.286 m, respectively. The anode geometry outside the magnetron, leading to the inlet and pmc boundaries, is designed to intercept leakage current.

The radii of shallow and deep cavities are respectively r_1=0.125 m and r_2=0.162 m, with corresponding depths of d_1=0.028 m and d_2=0.065 m, respectively. The depth ratio of the cavities is defined as $\rho=d_2/d_1$ and equals 2.32 for the N14 as shown in Fig. 1.

The dispersion relation is calculated using a standard Floquet harmonic analysis,[17] so we only outline the details here. It is assumed that a characteristic mode is dominated by the field components E_r, E_θ, and B_z, with the remaining components approximately 0. Then, for example, the expression for the θ component of the vector potential (A_θ) between the anode and cathode (AK-gap) has the form

$$A_{\theta n}(r,\theta,z,t) = \sum_{l=1}^{\infty}\sum_{m=-\infty}^{\infty} A_{lm}F_{lm}(r)\sin\left(\frac{l\pi z}{L_a}\right)e^{iM(m)\theta}e^{-i\omega t}, \tag{1}$$

where the $F_{lm}(r)$ are a combination of Bessel functions, ω the angular oscillation frequency, the azimuthal harmonic number[18] M is given by

$$M(m) = n + m(N/2), \tag{2}$$

and $|n| = 0, 1, 2, \ldots$, which specifies the mode number and its azimuthal symmetry.

There is an expression similar to Eq. (1) for A_m that has a form which makes the divergence of **A** equal to zero. Expressions for the field components are obtained through the appropriate derivatives of **A**. Applying matching conditions to the standing wave fields in the cavities leads to the dispersion relation.

The dispersion relation for the N14 configuration is shown in Fig. 2. It is infinitely periodic in the mode number n, and there are an infinite number of pass-bands. The dotted line corresponds to the 1st pass-band of the equivalent uniform cavity structure. Solid lines represent the lowest frequency pass-bands of the rising-sun. Symbols mark the frequencies of allowed modes. Only one period of the dispersion relation is shown.

Because a rising-sun is a bi-periodic structure the dispersion relation exhibits two periodicities; one is related to the angular separation between like cavities, and the second is due to the angular separation of each cavity.[16] Thus, the n=7 mode can be referred to as either the π-mode of the overall structure (fields 180 degrees out of phase in adjacent cavities) or the 2π-mode of the configuration of like cavities (fields in phase in like cavities). We refer to all modes relative to the overall periodicity.

The bi-periodic nature of the rising-sun causes the 1st pass-band (of a uniform cavity structure) to split into upper and lower frequency pass-bands. The most efficient mode in the rising-sun is the upper frequency n=7 mode. The frequency and phase velocity separation that occurs between the n=6 and n=7 modes reduces the risk of mode competition in the magnetron. However, when the cavity depth ratio is large, which further increases the n=6,7 frequency separation, mode competition from the n=3,4 modes can be just as severe. The upper frequency n=6 mode is the dominant competing mode in simulations.

When n=7 in Eq. (2), as for the π-mode, it is possible to have M=0. This azimuthal spatial harmonic is commonly referred to as the 0-harmonic of the π-mode.[16] It has the same oscillation frequency as the π-mode, because it is a spatial harmonic, and is the result of unequal rf currents in shallow and deep cavities. Inspection of Eq. (2) reveals that the 0-harmonic is uniform in θ. Therefore, every half cycle of oscillation the 0-harmonic fields either add to or subtract from the π-mode fields. We use this fact to obtain the 0-harmonic field amplitudes from simulation. This is accomplished by averaging the desired field component in 2π at every time step, in which case all other π-mode harmonics average to 0. The result is the amplitude of the 0-harmonic field superimposed on the applied field.

Early on in magnetron development the rising-sun configuration was invented to achieve mode stability. It was soon discovered that 0-harmonic contamination could have negative effects on magnetron performance, which led to the concept of strapping.[18] Conventional strapping techniques are not feasible for operation at high voltage. Consequently much relativistic magnetron work has involved rising-sun configurations. We show below that 0-harmonic contamination is particularly severe at relativistic voltages, and may be the major limiting factor in obtaining high efficiency from rising-sun configurations operated at high voltage.

III. 3D PIC SIMULATION AND RESULTS

A. 0-Harmonic contamination in the N14 rising-sun

The N14 configuration depicted in Fig. 1 was designed specifically for this study; the logic being to work with an experimentally practicable configuration of unknown performance characteristics and through 3D PIC simulation make predictions pertaining to its limitations and the associated causes, which could then be validated in a follow-on experiment. Dimensions were provided in the previous section.

The most significant departure from reality in this design is that the cathode is extended to the downstream boundary by a smaller radius (0.05 m) conducting cylinder where it is terminated in an open circuit. [This is the pmc (perfect magnetic conductor) boundary in Fig. 1(a)]. Normally the open circuit would occur at the end of the emitting part of the cathode, labeled cathode in Fig. 1(a), but this would add the axis (r=0) to the simulation, which would preclude using cylindrical coordinates (due to infinitesimally small cells in θ near the axis) and force approximating the geometry using cartesian coordinates. Including the open circuit is important from the dc standpoint, and tests show that overall results are not dependent on the location of the pmc. Thus, the Fig. 1 configuration in cylindrical coordinates is the preferred model.

The magnetron is driven by a dc, TEM (transverse electromagnetic) voltage pulse injected at the inlet [Fig. 1(a)]. The temporal profile of the injected voltage is plotted in Fig. 3.

The starting point for simulations is the N14 with depth ratio equal to 2.32, which runs in the n=7 mode with frequency f=1052 MHz, voltage=492 kV, impedance=22 Ω, and efficiency=21%. The injected voltage amplitude and applied magnetic field are V_{in}=400 kV and B_{z0}=1.6 kG.

In order to investigate effects of the 0-harmonic one must be able to vary its magnitude. This is accomplished by decreasing the cavity depth ratio (ρ defined above) while keeping the average cavity radius constant. However, when the depth ratio becomes small enough the mode of oscillation switches from n=7 to n=6 with a significant decrease in efficiency. To overcome this difficulty we apply a pre-excitation signal that begins in the risetime of the voltage pulse. A π-mode distribution for E_θ is set up across the entrances to all cavities ($r=r_a$) at the axial midplane of the anode and is allowed to grow to approximately 10% of the expected saturated value, at which time it is turned off (about 11 cycles). This is sufficient to lock the phase of oscillation in the desired mode. The pre-excitation window is delineated by vertical dotted lines in Fig. 3. (Note that pre-excitation only affects the growth of the mode and not its final amplitude; that is, efficiency is not affected either.)

The frequency of the pre-excitation signal is determined by cold testing the exact structure using QUICKSILVER. The electron flow contributes to the loading (discussed in more detail below), which reduces the operating frequency by as much as 100 MHz relative to the cold frequency. It is necessary to subtract this amount from the cold frequency to get the correct pre-excitation frequency.

It was pointed out in Sec. II that extraction through irises in every other cavity creates a rising-sun. Consequently there is 0-harmonic contamination even when all cavities have the same depth. To completely eliminate this effect required inverting the rising-sun structure. In this case the depth ratio is less than 1 and power is extracted from shallow cavities. It was necessary to use pre-excitation to get the π-mode in all inverted configurations.

To get an initial operating point for a given configuration in simulations we use the Hull cutoff and relativistic Buneman-Hartree conditions[19] to estimate the magnitude of the applied magnetic field (B_{z0}) based on a desired operating voltage. If necessary B_{z0} is varied until the π-mode is obtained. The operating point shown in Fig. 4 is the result of this procedure for the N14 with $\rho=2.32$.

Unless stated otherwise the operating point, in addition to all other quantities of interest, is determined in the steady state of oscillation. Simulation data are provided in Fig. 5 for the highest efficiency N14 configuration, which is an inverted structure with $\rho=0.57$ and pre-excitation. In this case V_{in}=400 kV and B_{z0}=1.55 kG. Operating voltage and net current, Fig. 5(a), are used to calculate input power and impedance. The integral of E_θ in θ across the cavity gaps yields rf voltages, Fig. 5(b), which in turn are used to calculate the frequency spectrum and obtain the oscillation phase. The time average of the total integrated Poynting flux from all outlet boundaries [see Fig. 1(a)] yields the rms output power, Fig. 5(c), which is used in conjunction with the input power to obtain total efficiency (η). Electronic efficiency (η_e) is given by $\eta_e = 100[1-\overline{KE}/(eV)]$, where V is the operating voltage, and $\overline{KE}$, the average kinetic energy of electrons that reach the anode block in the cavity region, is calculated by averaging over the corresponding distribution function. (Note that η is generally less than η_e due to power losses on the cathode and through leakage current.)

The mode of oscillation can often be determined from particle plots. For a single mode the number of spokes is equal to the absolute value of the mode number n. This is illustrated for the n=7 and most dominant competing mode, n=6, in the N14 rising-sun, Figs. 6(a) and 6(b), respectively.

The maximum value of η is determined by increasing the iris openings (in z) until mode competition and/or switching prevents any further increase. Because the oscillation frequency decreases with increasing iris width, slight increases in B_{z0} are often necessary to maintain the π-mode. Figure 7 contains plots of η and cold cavity Q versus iris width corresponding to the inverted N14 with ρ=0.57. The vertical dotted line marks the threshold beyond which further increases in iris width results in loss of the n=7 mode and reduction in efficiency. This behavior is characteristic of all magnetron configurations we have simulated.

The threshold iris width in this case corresponds to 0.37λ (free space wave length for f=1099 MHz). Maximum possible power for this type of iris should be radiated when its width is about 0.5λ (about 13.6 cm). Linearly extrapolating the efficiency line in Fig. 7 to 13.6 cm suggests that approximately 58% total efficiency would be possible without mode competition. This is more in line with commercial magnetron efficiency.

We observe that the location of the threshold for mode competition exhibited in Fig. 7 depends on conditions in the magnetron. In particular we find that 0-harmonic contamination and space charge intensity decrease the value of the threshold iris width, thereby lowering the maximum possible efficiency.

By varying ρ we determine the effect of the 0-harmonic on efficiency. Figure 8 contains plots of the normalized 0-harmonic B_z (relative to B_{z0}) and total efficiency versus cavity depth ratio ρ. The maximum total efficiency was obtained by generating data similar to Fig. 7 for each value of ρ. Figure 8 suggests that the decline in efficiency with increasing ρ is well correlated with the increasing degree of 0-harmonic contamination. Substantially reducing the 0-harmonic fields by inverting the rising-sun structure (as described above) increases the efficiency by a factor of 1.75. (Note that pre-excitation was necessary to get the π-mode for $\rho \leq 1$).

In the N14 with ρ=2.32 the amplitude of the 0-harmonic B_z is large. This is shown in Fig. 9, which is a plot of the 0-harmonic component of B_z versus time at a location corresponding to r=0.085 m and the axial midplane of the cavities. The dashed line represents B_{z0} and the dotted line is the local, net, dc magnetic field, which is less than B_{z0} due to diamagnetic effects. Since the average value of B_z effects both insulation and synchronism at a given voltage, it should not be surprising that a large variation about the average degrades magnetron performance. This is exhibited quantitatively in Figs. 10 and 11.

Figure 10 shows the variation of the average magnetic field about the operating point for the two extreme cases in Fig. 8 (ρ=0.57 and ρ=2.32). The inverted structure in which the 0-harmonic has small amplitude shows little variation about synchronism [Fig. 10(a)]. In contrast, the case with $\rho=2.32$, Fig. 10(b), exhibits a large variation about synchronism, to the extent that insulation is completely lost on the half cycle in which the 0-harmonic B_z reduces the average field. In this case the electronic efficiency is 0. During the next half cycle the 0-harmonic B_z increases the average field, which increases efficiency. However, this cannot overcome the negative effects that occur during the previous half cycle, and the net result is reduced efficiency.

Figure 11 illustrates the loss of insulation due to large 0-harmonic B_z. The solid curve in each figure represents the electron power contained in all spokes incident on the anode block in the interaction region as a function of time. Each peak represent one-half cycle of the oscillation, during which time all spokes are lost to either deep or shallow cavities (in the n=7 mode). Superimposed on this is the amplitude of the 0-harmonic B_z.

Figures 11(a) and 11(b) correspond to the two extreme cases in Figs. 8 and ~~11~~ 10, $\rho=0.57$ and $\rho=2.32$, respectively. For small 0-harmonic amplitude, Fig. 11(a), the spoke power loss is approximately the same in both deep and shallow cavities. In contrast, for large 0-harmonic amplitude, Fig. 11(b), a disproportionate amount of power is lost to one set of cavities when the average magnetic field is reduced and insulation is lost. We have determined that the excess power is lost in the open (deep) cavities. In addition to a degradation in efficiency, this could also produce plasma in deep cavities due to excessive electron bombardment of the anode.

B. The N22 magnetron and space-charge effects

In simulations of the N14 we observed that efficiency increased when the operating impedance was increased at fixed voltage, and vice versa. In addition, the departure of the operating frequency from the cold frequency is observed to increase with increasing current in the interaction region. This behavior suggests that the intense space charge produced at relativistic voltages significantly contributes to the total Q (i.e. the loading) of the magnetron, which would lower the threshold Q at which mode competition begins (as discussed above).

To test this hypothesis we scaled the N14 to larger diameter in an attempt to get a magnetron that runs at about the same voltage and impedance, but with reduced current density (due to the larger diameter). The result is the 22 cavity, cylindrically symmetric, N22 magnetron. The geometry is shown schematically in Fig. 12, in which three particle plots are used to illustrate various cross sections and cathode configurations. Figure 12(a) is a cross section in the rθ plane. Figure 12(b) is a cross section in the rz plane though a cavity that contains an iris. Power is extracted from every other cavity.

Due to the increased size of the problem (relative to the N14) only half the axial length of the geometry was simulated. The right boundary in Fig. 12(b) corresponds to the symmetry midplane. In this case power flow into the problem is symmetric, which does not have a significant effect on efficiency relative to a configuration like the N14.

The cathode radius and axial length are r_c=0.1533 m and L_c=0.3668 m, respectively. The anode inner radius and axial length are r_a=0.183 m and L_a=0.4668 m, respectively. The anode geometry outside the magnetron, leading to the inlet and pmc boundaries, is designed to intercept leakage current [as shown in Fig. 12(b)].

All cavities are uniform with radii r_1=r_2=0.2354 m, and with corresponding depths of d_1=d_2=0.0524 m. Although not a rising-sun, the N22 has an effective depth ratio of about 1.3, which is side effect of the power coupling scheme. Consequently, there is a small amplitude 0-harmonic that is about 15% of B_{z0}.

For V_{in}=300 kV and B_{z0}=1.3 kG the N22 operating parameters are: V=429 kV, impedance=17.7 Ω, phase=π (n=11), f=950 MHz, output power=3.4 GW, η=32.2%, and η_e=60.2%. Pre-excitation was necessary to get oscillation in the π-mode. It was applied in the manner described in the previous section.

Figure 12(b) shows that electrons leak out of the interaction region along magnetic field lines. In this case (compared to the N14) the leakage power is a substantial fraction of the input power (~30%). To reduce the power loss through leakage an alternative cathode geometry with focusing endcaps was tried. In addition, to increase impedance the cathode length is reduced by 0.1333 m to L_a=0.2335 m. This slightly different configuration is shown in Fig. 12(c), and reduces the fraction of leakage power to about 8.3%. Operating parameters are: V=456 kV, impedance=22.4 Ω, phase=π (n=11), f=951 MHz, output power=3.7 GW, η=39.7%, and η_e=53.8%. Stopping the leakage current increased the total efficiency, but produced a decrease in the electronic efficiency. Figure 13 suggests an explanation for this result.

Figure 13 is a plot of the total efficiency (η) and electronic efficiency (η_e) versus electron current density in the interaction region for the N22 with cathode configurations shown in Figs. 12(b) and 12(c). An average value of current density is obtained by dividing the electron current returning to the anode in the interaction region by the emitting surface area. This number is used to quantify space charge intensity.

Figure 13 suggests that electronic efficiency decreases with increasing space charge intensity. We speculate that the mechanism for this is spoke expansion due to space charge forces. This would force more electrons into less efficient orbits relative to a reduced space charge case. Thus, cutting off leakage current put more electron power in the interaction region, which explains the increase in total efficiency, but leads to a reduction in electronic efficiency due to increased space charge intensity. (To precisely verify this using PIC simulation requires tracking orbits for individual particles, which is not available at this time.)

The effect of space charge intensity on efficiency is more pronounced in a comparison of different magnetrons with similar operating voltages. Figure 14 is a plot of average current density (as calculated above), η, and η_e versus cathode radius from simulations of three different magnetrons; the N14, N22, and the A6.[11] Points with the same cathode radius represent results for the same magnetron. The peak efficiency of each magnetron occurs at approximately the same voltage (V~400 kV ± 50 kV). Figure 14 suggests that efficiency increases with increasing cathode radius due to a reduction in space charge intensity, which is a consequence of the enlarged surface area over which emission occurs.

IV. CONCLUSIONS

A gigawatt class, relativistic magnetron (V~500 kV) requires many kiloamperes of current to produce this power, even at modest conventional efficiency (~50%). The results of this study suggest that achieving this level of efficiency at relativistic voltages is a matter of mode control, which we show can be accomplished through minimizing both space charge intensity and 0-harmonic contamination.

These requirements, however, suggest opposing design constraints. Minimizing space charge intensity while maintaining high power requires the magnetron diameter to be large to enable a large cathode emission area. Consequently the anode block contains many cavities and therefore requires a technique for mode control. Although the rising-sun is the most practicable, conventional design for mode control at relativistic voltages, achieving mode stability requires a large cavity depth ratio which causes significant 0-harmonic contamination. Simulation suggests this unnecessarily reduces the maximum efficiency possible at a given operating voltage. Thus, achieving conventional efficiency in relativistic magnetrons may require developing a nonconventional strapping technique that is feasible at high voltage, and which might also be used in combination with injection locking.

AKNOWLEDGMENTS

This work was sponsored by the United States Air Force Research Laboratory, Directed Energy Directorate, Kirtland AFB, NM, and Sandia National Laboratories, NM. Sandia is a multiprogram laboratory operated by Sandia Corporation, a Lockheed Martin Company, for the US Department of Energy under Contract DE-ACO4-94AL85000.

REFERENCES

[1] George B. Collins, *Microwave Magnetrons* (McGraw-Hill, New York, 1948).

[2] A. M. Clogston, in *Microwave Magnetrons*, edited George B. Collins (McGraw-Hill, New York, 1948) pp. 401-402

[3] T. A. Treado, R. A. Bolton, T. A. Hansen, P. D. Brown, and J. D. Barry, IEEE Trans. Plasma Sci. 20(3), 351 (1992).

[4] J. Benford and J. Swegle, *High-Power Microwaves* (Artech House, Boston, 1992) pp. 147-180.

[5] J. Benford, in *High Power Microwave Sources*, edited by Victor L. Granatstein and Igor Alexeff (Artech House, Inc., Boston, 1987), pp. 351-395.

[6] A. Palevsky and G. Bekefi, Phys. Fluids 22(5), 986 (1979).

[7] H. Sze, B. Harteneck, J. Benford, and T. S. T. Young, IEEE Trans. Plasma Sci. 15(3), 327 (1987).

[8] J. Benford, H. Sze, T. Young, D. Bromley, and G. Proulx, IEEE Trans. Plasma Sci. 13(6), 538 (1985).

[9] T. A. Treado, W. O. Doggett, G. E. Thomas, R. S. Smith III, J. Jackson-Ford, and D. J. Jenkins, IEEE Trans. Plasma Sci. 16(2), 237 (1988).

[10] J. S. Levine, B. D. Harteneck, and H. D. Price, in *Intense Microwave and Particle Beams*, edited by H. E. Brandt, Proceedings SPIE 2557 (SPIE, Bellingham, 1995), pp. 74-79.

[11] R. W. Lemke, T. C. Genoni, and T. A. Spencer, Phys. Plasmas 6(2), 603 (1999).

[12] W. Arter and J. W. Eastwood, IEEE Trans. on Plasma Sci. 26(3), 714 (1998).

[13] D. B. Seidel, M. L. Kiefer, R. S. Coats, T. D. Pointon, J. P. Quintenz, and W. A. Johnson, in *The CP90 Europhysics Conference on Computational Physics*, edited by Armin Tenner (World Scientific, Amsterdam, 1991), pp. 475-482.

[14] S. Millman and W. V. Smith, in *Microwave Magnetrons*, edited by George B. Collins (McGraw-Hill, New York, 1948) pp. 470-481.

[15] A. M. Clogston, in *Microwave Magnetrons*, edited by George B. Collins (McGraw-Hill, New York, 1948) pp. 419-434.

[16] N. Kroll, in *Microwave Magnetrons*, edited by George B. Collins (McGraw-Hill, New York, 1948) pp. 83-117.

[17] R. E. Collin, *Foundations for Microwave Engineering* (McGraw-Hill, New York, 1966) p. 475.

[18] G. B. Collins, in *Microwave Magnetrons*, edited by George B. Collins (McGraw-Hill, New York, 1948) pp. 32-35.

[19]R. V. Lovelace and T. F. T. Young, Phys. Fluids 28(8), 2450 (1985).

FIGURE CAPTIONS

Fig. 1. Schematics of N14 rising-sun for PIC simulation study in (a) rz plane of a deep cavity, (b) $r\theta$ plane at z=0.3 m, and (c) $r\theta$ plane at z=0.4 m (along a line that includes an extraction iris). B_{z0} represents the applied magnetic field. Power is radiated through an iris located at the end of every deep cavity.

Fig. 2. Dispersion relation for TE waves in the N14 rising-sun. Dashed line is for uniform cavities with radii equal to average radius of rising-sun.

Fig. 3. Voltage wave form used in 3D simulations. Vertical dashed lines bound temporal window in which pre-excitation is applied when necessary to get π-mode oscillation.

Fig. 4. Plot of the Hull voltage and Buneman-Hartree voltages versus applied magnetic field showing the operating point for N14 rising-sun with cavity depth ratio=2.32. This also represents the condition for synchronism in the magnetron; that is, when the electron drift velocity is equal to the wave phase velocity.

Fig. 5. Simulation data for an inverted (depth ratio=0.57) N14, which requires pre-excitation and is the most efficient 14 cavity configuration simulated. (a) Operating voltage and current, (b) example of an rf voltage across the entrance to one cavity, (c) input and output rms power used to obtain total efficiency, and (d) kinetic energy distribution function for electrons impinging on the anode block, which is used to calculate electronic efficiency. Qualitatively these plots are typical of all magnetron configurations when oscillating in the π-mode.

Fig. 6. Particle plots in an $r\theta$ plane that includes the irises for the N14 rising-sun. (a) Spoke configuration for the π-mode (n=7). (b) Spoke configuration for the predominant competing mode (n=6).

Fig. 7. Plot of cold cavity Q and total efficiency versus iris width for the N14 with cavity depth

ratio=0.57. This data illustrates the procedure for optimizing the magnetron for power and efficiency. The vertical dotted line represents a threshold in iris width (or Q) beyond which mode competition prevents any further increase in efficiency.

Fig. 8. Normalized 0-harmonic B_z amplitude and total efficiency versus cavity depth ratio for the N14 configuration.

Fig. 9. 0-Harmonic of B_z versus time for the N14 with depth ratio=2.32. The horizontal dashed and dotted lines are respectively the applied magnetic field (B_{z0}) and the local average magnetic field. They are not equal due to diamagnetic effects.

Fig. 10. Plots of operating voltage versus applied magnetic field (B_{z0}) showing the effect that the 0-harmonic of B_z has on synchronism (the operating point) for the N14 with depth ratios (a) 0.57 and (b) 2.32. In (b) the 0-harmonic causes substantial variation about synchronism, and reduces the average magnetic field to the extent that insulation is lost.

Fig. 11. Spoke power incident on anode (solid curves) and 0-harmonic B_z (dashed curves) versus time for the N14 magnetron with depth ratios (a) 0.57 and (b) 2.32. In (b) excessive spoke power loss occurs when the 0-harmonic B_z reduces the average magnetic field below the insulation threshold, as suggested by Fig. 10(b).

Fig. 12. Particle plots for the N22 magnetron illustrating the geometry, and the π-mode (n=11) electron flow. (a) $r\theta$ plane that includes an extraction iris. (b) rz plane showing electrons leaking out of the interaction region along magnetic field lines. (c) rz plane for an alternative cathode geometry that uses electrostatic focussing endcaps to reduce leakage current.

Fig. 13. Total efficiency versus average current density in the interaction region for the N22 configurations depicted in Figs. 12(b), no cathode endcaps, and 12(c), with cathode endcaps (reduced leakage points).

Fig. 14. Total efficiency (η), electronic efficiency (η_e), and average current density in the interaction region versus cathode radius for the A6, N14, and N22 magnetrons. Efficiency increases with increasing cathode radius due to the reduction in space charge intensity.

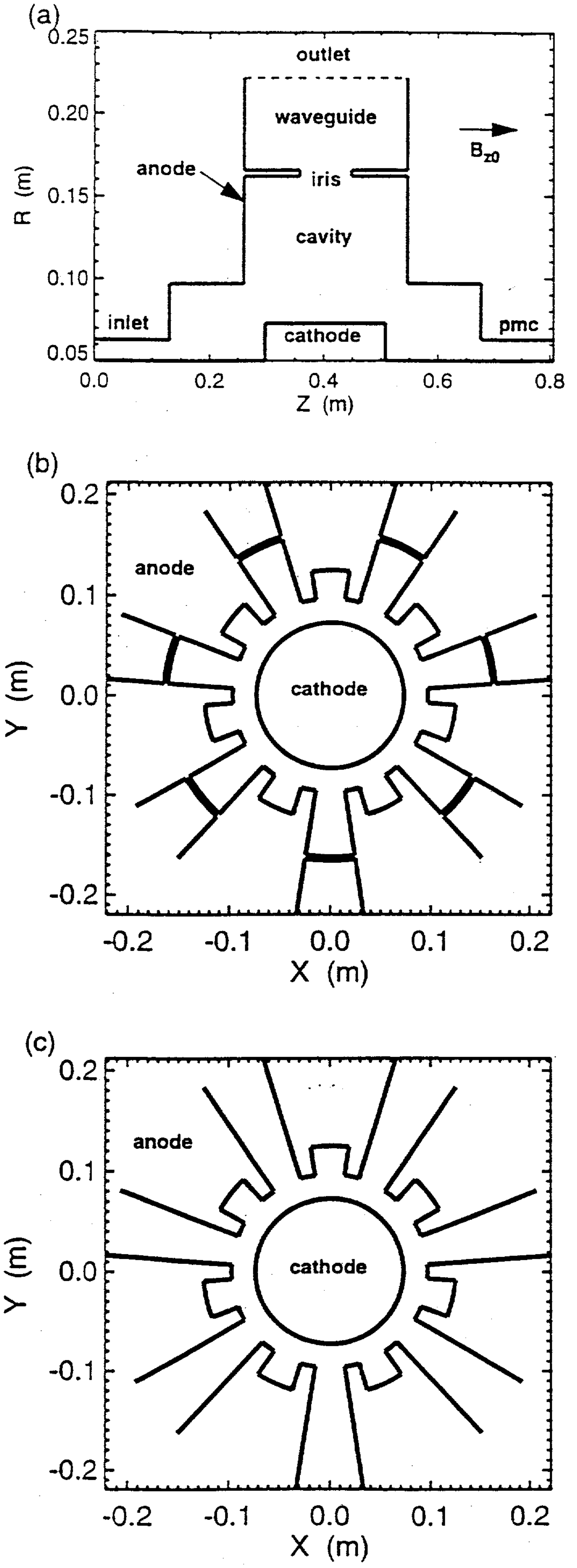
(a)
outlet
waveguide
anode
iris
cavity
inlet
cathode
pmc
B_{z0}
R (m)
0.25
0.20
0.15
0.10
0.05
0.0
0.2
0.4
0.6
0.8
Z (m)
(b)
anode
cathode
Y (m)
0.2
0.1
0.0
-0.1
-0.2
-0.2
-0.1
0.0
0.1
0.2
X (m)
(c)
anode
cathode
Y (m)
0.2
0.1
0.0
-0.1
-0.2
-0.2
-0.1
0.0
0.1
0.2
X (m)

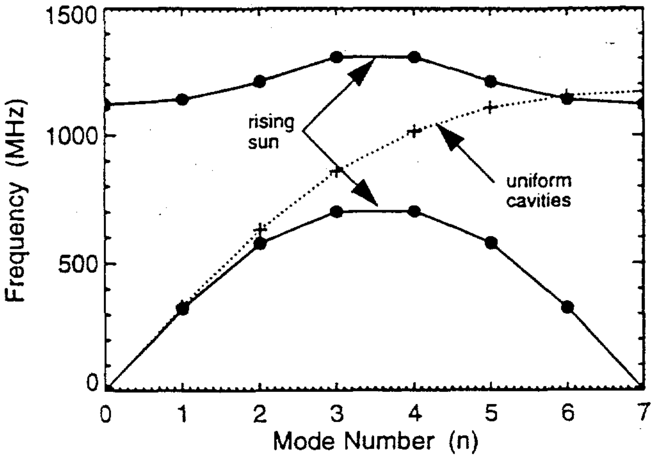

Figure 2, R.W. Lemke Physics of Plasmas

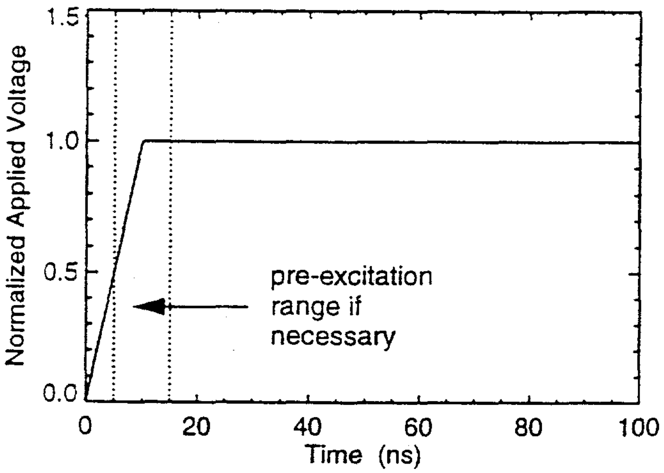

Figure 3, R.W. [illegible], Physics of Plasmas

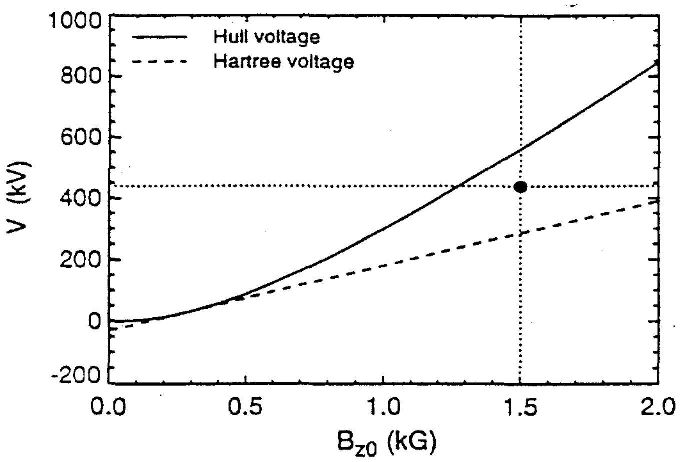

Figure 4, R. W. Lemke, Physics of Plasmas

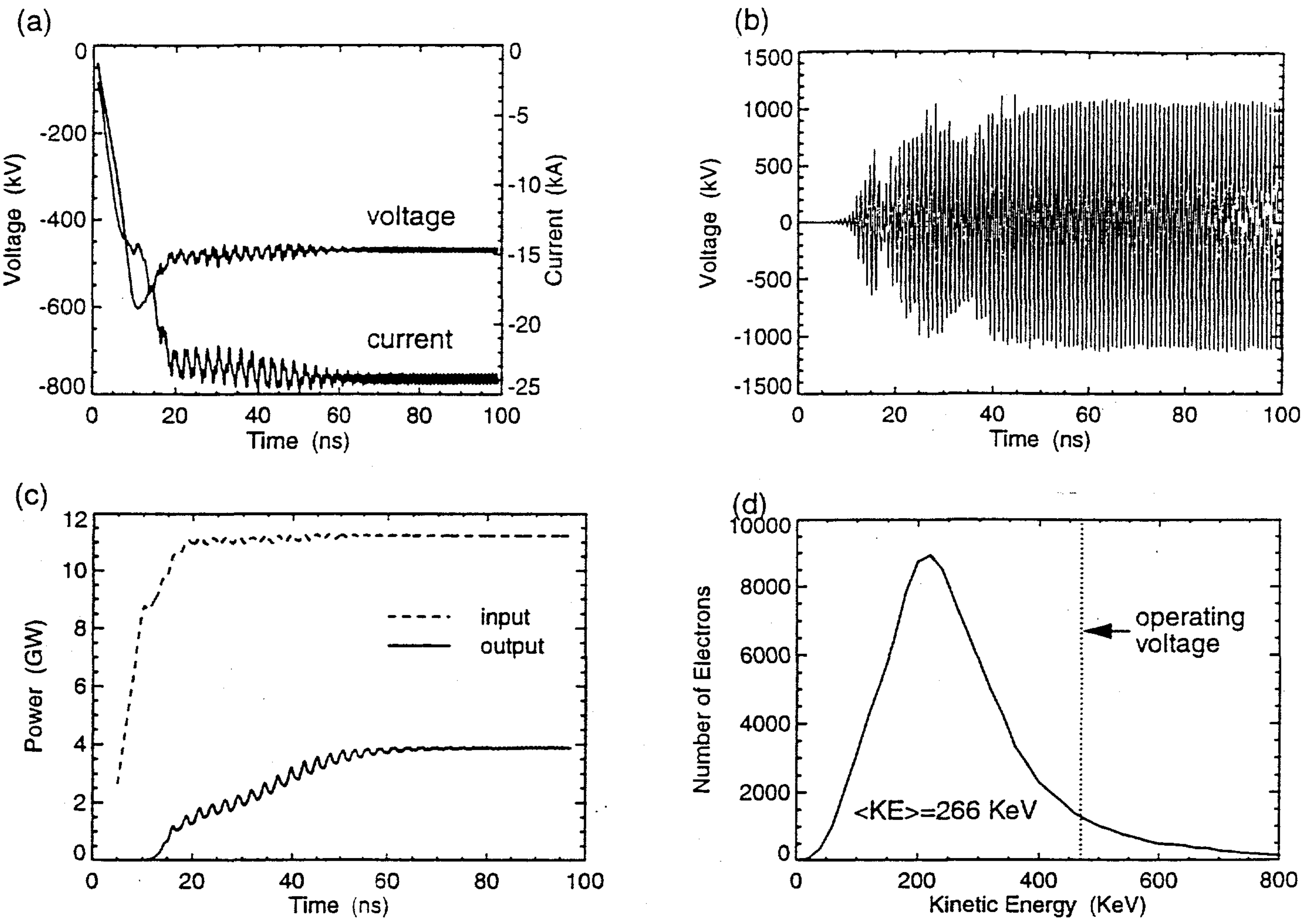

Figure 5, R.W. Lemke Physics of Plasmas

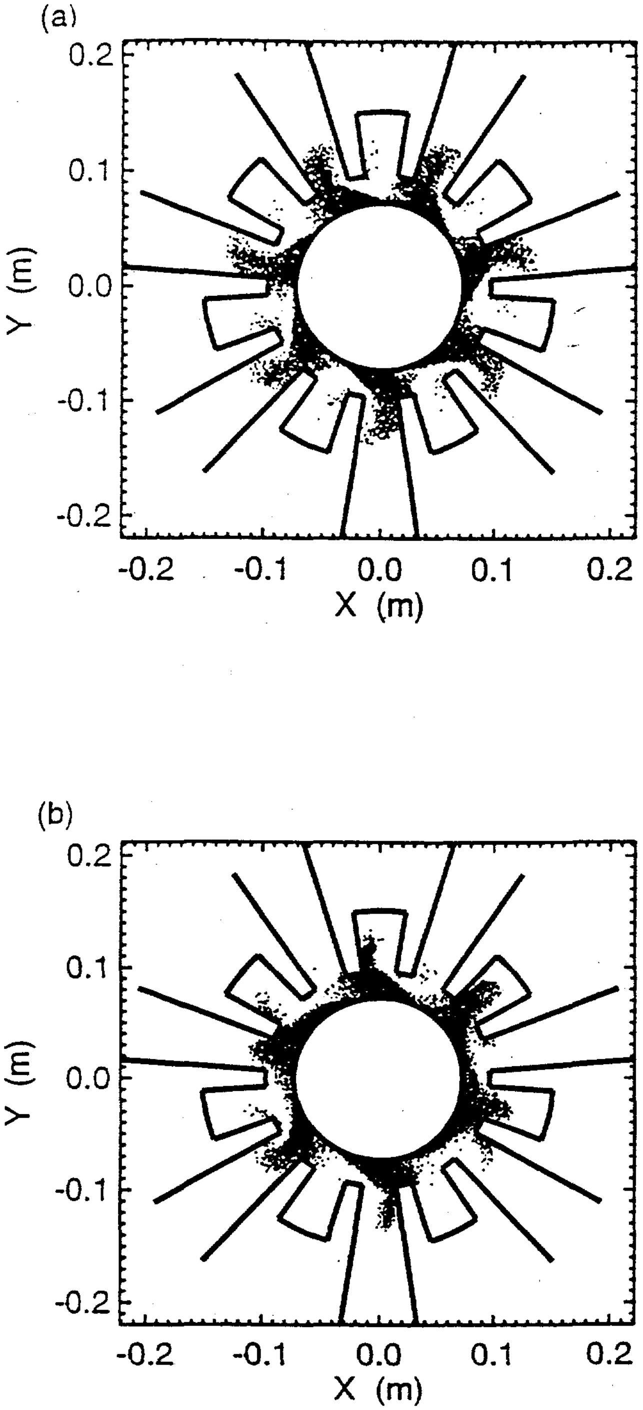

Figure 6, R.W. Linke, Physics of Plasmas

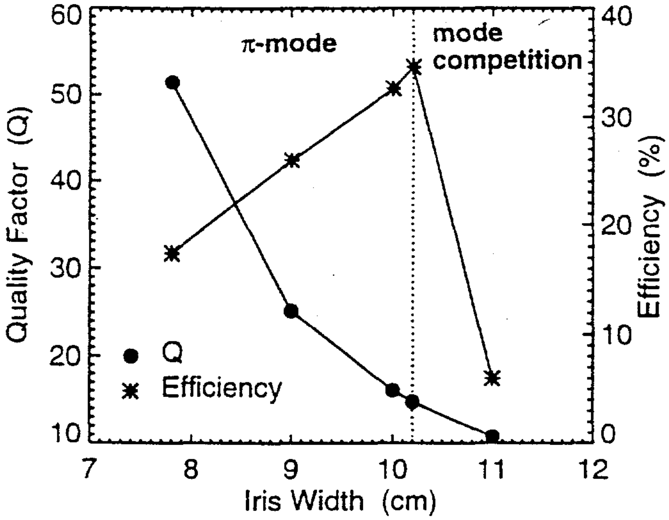

Figure 7, R.W. Lemke, Physics of Plasmas

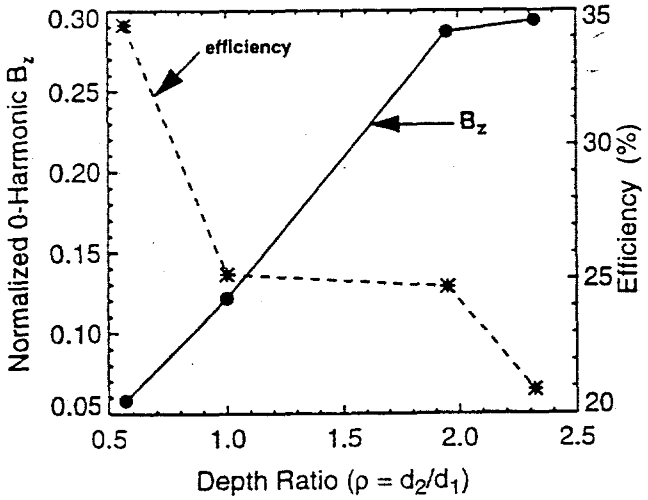

Figure 8, R. W. Lemke, Physics of Plasmas

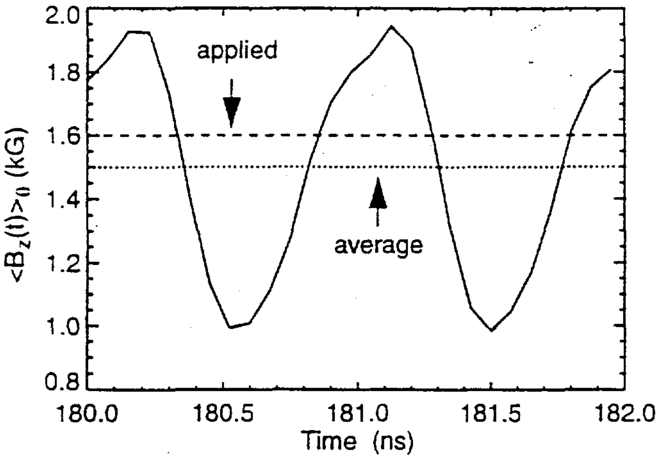

Figure 9, R.W. Lemke, Physics of Plasmas

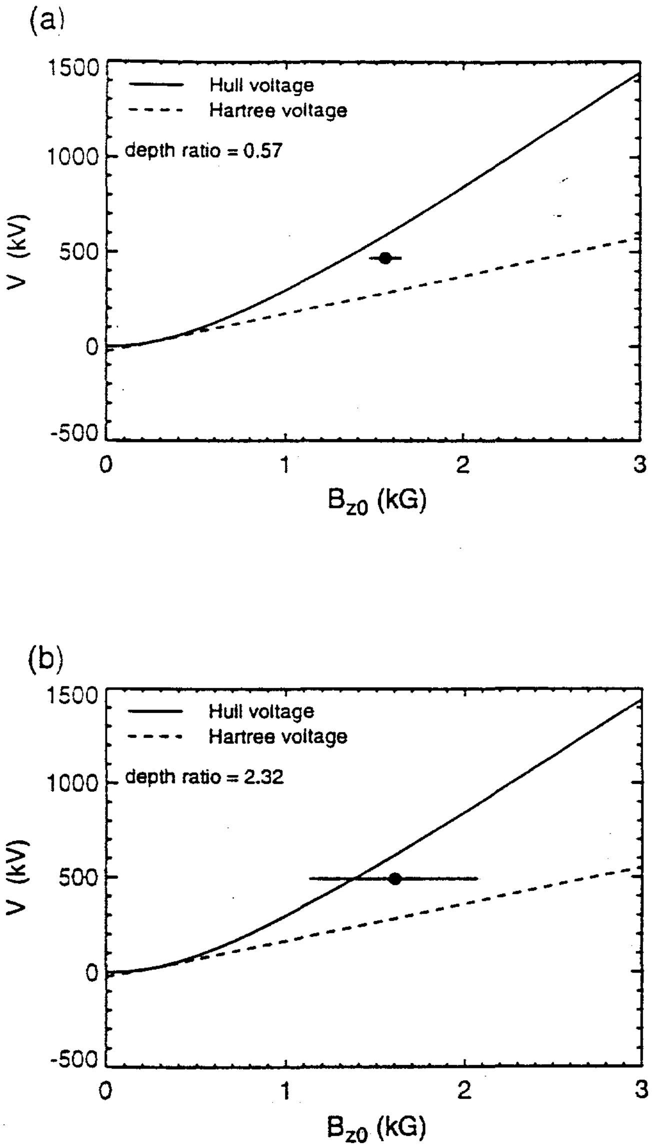

Figure 10, R.W. Lemke, Physics of Plasmas

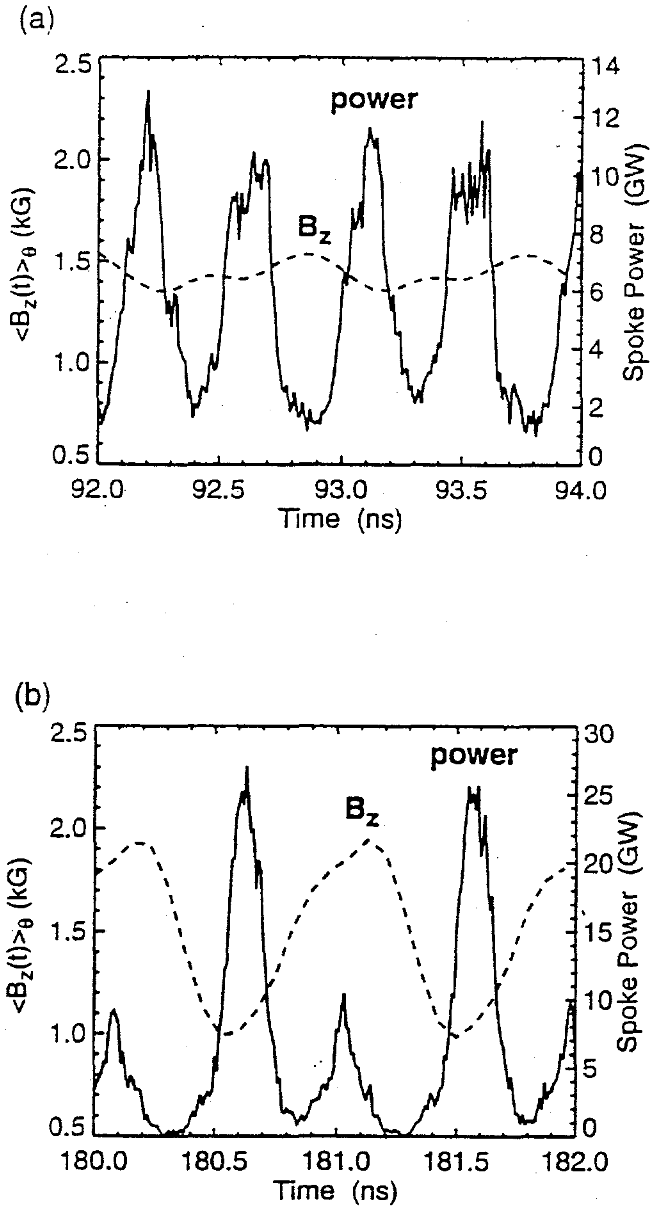

Figure 11, R.W. Lemke, Physics of Plasmas

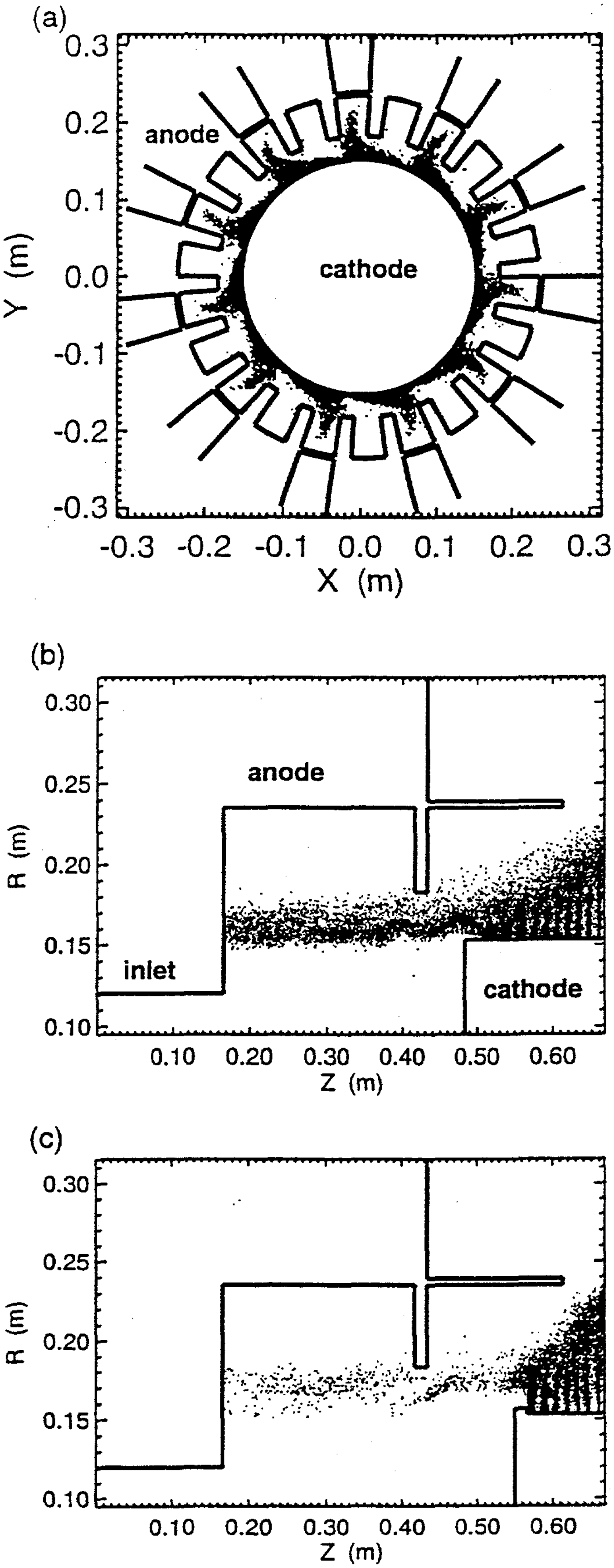

Figure 17 R. W. Lemke Physics of Plasmas

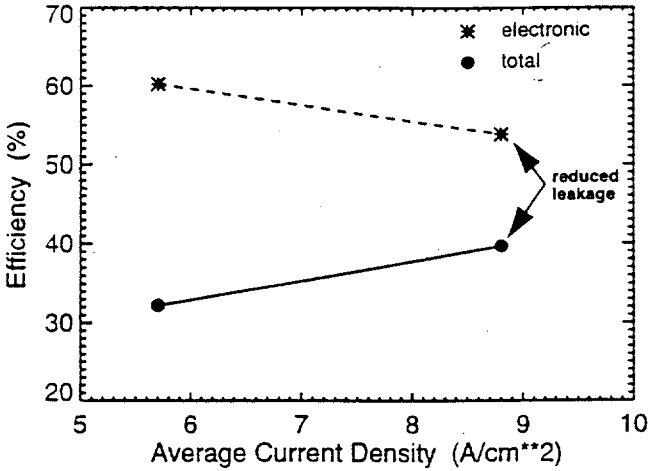

Figure 13, R.W. Lemke, Physics of Plasmas

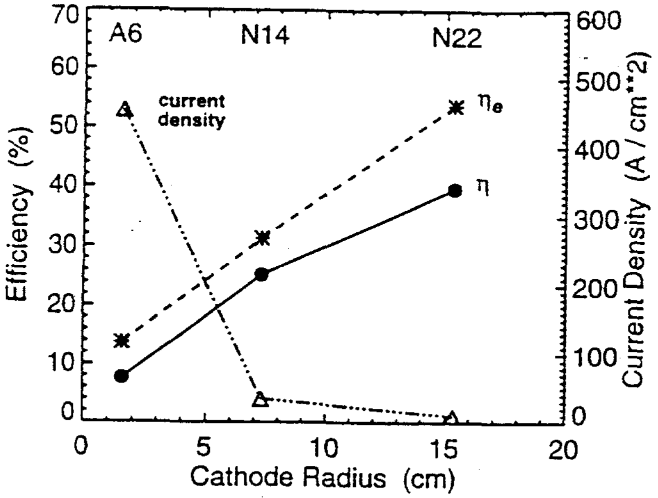

Figure 14, R.W. Lemke, Physics of Plasmas